

# Beyond Chainmail: Computational Modeling of Discrete Interlocking Materials

PENGBIN TANG, Université de Montréal, Canada and ETH Zürich, Switzerland

STELIAN COROS, ETH Zürich, Switzerland

BERNHARD THOMASZEWSKI, ETH Zürich, Switzerland

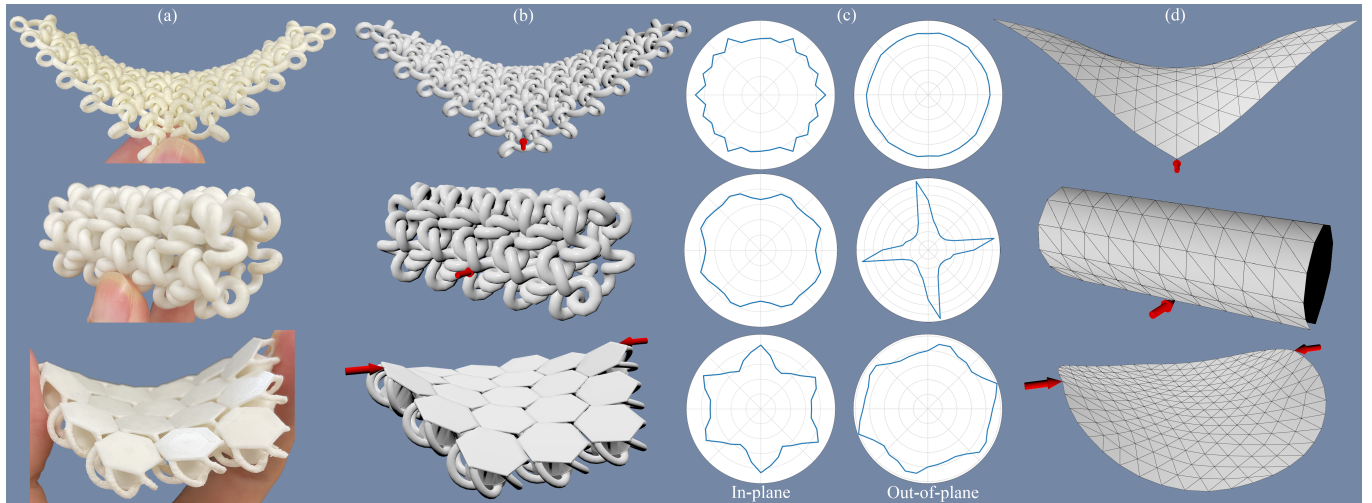


Fig. 1. Discrete Interlocking Materials are governed by strongly coupled, highly anisotropic, and asymmetric deformation limits. Our method is able to capture and reproduce these effects for many types of interlocking materials (a). Using native-scale simulations as a basis (b), we construct macromechanical deformation limits on bending and stretching (c) which we use to develop an efficient macro-scale simulation model (d).

We present a method for computational modeling, mechanical characterization, and macro-scale simulation of discrete interlocking materials (DIM)—3D-printed chainmail fabrics made of quasi-rigid interlocking elements. Unlike conventional elastic materials for which deformation and restoring force are directly coupled, the mechanics of DIM are governed by contacts between individual elements that give rise to anisotropic deformation constraints. To model the mechanical behavior of these materials, we propose a computational approach that builds on three key components. (a): we explore the space of feasible deformations using native-scale simulations at the per-element level. (b): based on this simulation data, we introduce the concept of strain-space boundaries to represent deformation limits for in- and out-of-plane deformations, and (c): we use the strain-space boundaries to drive an efficient macro-scale simulation model based on homogenized deformation constraints. We evaluate our method on a set of representative

discrete interlocking materials and validate our findings against measurements on physical prototypes.

CCS Concepts: • Computing methodologies → Physical simulation; Modeling methodologies; • Applied computing → Computer-aided design.

Additional Key Words and Phrases: Bi-Phasic Materials, Homogenization, Mechanical Characterization, Strain Limiting, Data-Driven Macromechanical Model.

## ACM Reference Format:

Pengbin Tang, Stelian Coros, and Bernhard Thomaszewski. 2023. Beyond Chainmail: Computational Modeling of Discrete Interlocking Materials. *ACM Trans. Graph.* 42, 4 (August 2023), 12 pages. <https://doi.org/10.1145/3592112>

## 1 INTRODUCTION

Designing materials with desired mechanical properties is an important problem in science and engineering. Often, designers must create materials whose flexibility allows for proper functioning while providing the strength needed to prevent excessive deformation and support external loads. For conventional elastic materials, reconciling these soft-stiff requirements means designing for strong nonlinearities—and with increasing stiffness contrast, this task becomes ever more challenging. Here we consider a new class of Discrete Interlocking Materials (DIM): generalized chainmail fabrics made of quasi-rigid interlocking elements. Unlike conventional elastic materials for which restoring force increases in lockstep

Authors' addresses: Pengbin Tang, Université de Montréal, Canada and ETH Zürich, Switzerland, pengbin.tang@umontreal.ca; Stelian Coros, ETH Zürich, Switzerland, stelian@inf.ethz.ch; Bernhard Thomaszewski, ETH Zürich, Switzerland, bthomasz@inf.ethz.ch.

Permission to make digital or hard copies of all or part of this work for personal or classroom use is granted without fee provided that copies are not made or distributed for profit or commercial advantage and that copies bear this notice and the full citation on the first page. Copyrights for components of this work owned by others than the author(s) must be honored. Abstracting with credit is permitted. To copy otherwise, or republish, to post on servers or to redistribute to lists, requires prior specific permission and/or a fee. Request permissions from [permissions@acm.org](mailto:permissions@acm.org).

© 2023 Copyright held by the owner/author(s). Publication rights licensed to ACM. 0730-0301/2023/8-ART \$15.00 <https://doi.org/10.1145/3592112>

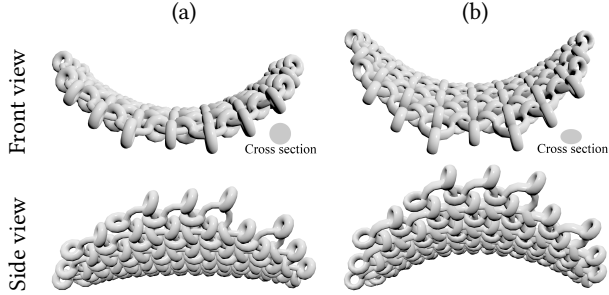


Fig. 2. Element cross-section determines coupling for bending. Two three-fold symmetric materials are bent using the same uniaxial load case. The elements of design (a) have circular cross-section, while cross-sections for design (b) are slightly ellipsoidal. This small asymmetry in geometry leads to much larger coupling between principal and orthogonal curvature.

with deformation, the mechanics of DIM is governed by contacts between individual elements. Their particular structure leads to extremely high contrast in deformation resistance: when contacts are sparse or unstructured, deformation is possible without any restoring force (the *slack* regime). Once a chain of contacts is formed along a given loading direction, further deformation is resisted with the full strength of the base material (the *taut* regime). This biphasic behavior lends DIM both strength and flexibility, making them attractive for use in robotics, orthotics, sportswear, and many other areas of application. To support such applications, however, we must predict the macro-mechanical behavior of DIM from their native-scale structure, i.e., element shape and connectivity. This relation is highly non-trivial as small changes in element shape can change the macromechanical behavior substantially (see Fig. 2).

In this work, we propose a computational approach for modeling and characterizing discrete interlocking materials composed of quasi-rigid elements. Rather than through the properties of their base material, we describe DIM through their strain-space boundaries that delineate the space of kinematically feasible configurations. These boundaries describe multi-dimensional, highly anisotropic limits for in- and out-of-plane deformations. In order to capture this complex mechanical behavior, we propose a novel homogenization approach for distilling macroscale deformation limits from native scale simulations. For each material, we perform thousands of virtual deformation tests for uni- and bi-axial stretching and bending in different directions. We thus establish a sample-based representation of a material's feasible set of deformations, from which we extract its strain-space boundary. We use this boundary to derive various metrics for characterization and to develop a homogenized model for DIM that combines thin-shell simulation with anisotropic deformation constraints for stretching and bending. Using this computational framework, we explore the space of discrete interlocking materials and characterize the macro-mechanical behavior of a diverse set of samples. Our simulation-based results are validated through real-world experiments, showing good agreement on both qualitative and quantitative levels. In summary, the key technical contributions of our work are

- the first formal framework for computational modeling and mechanical characterization of discrete interlocking materials,
- a method for homogenizing strain limits for in- and out-of-plane deformations,
- a representation of multi-dimensional deformation limits as feasible sets in strain space,
- a data-driven macromechanical model for discrete interlocking materials that combines thin shell simulation with homogenized deformation constraints.

## 2 RELATED WORK

*Metamaterial Design.* Through precisely architected microstructures, flexible metamaterials can achieve a broad range of macromechanical properties [Bertoldi et al. 2017]. Fueled by the increasing availability of 3D printing technology, the graphics community has started to embrace the problem of generating 3D-printable content such as models optimized for stability [Lu et al. 2014; Stava et al. 2012; Zhou et al. 2013], mechanical assemblies [Ceylan et al. 2013; Coros et al. 2013; Thomaszewski et al. 2014; Zhu et al. 2012], or characters that can be posed and deformed in desired ways [Bächer et al. 2012; Skouras et al. 2013]. One particular line of research in this context investigates the creation of 3D-printable metamaterials. The spectrum includes layered materials fabricated with multi-material printers [Bickel et al. 2010], materials with lattice-[Panetta et al. 2017, 2015], voxel- [Schumacher et al. 2015; Zhu et al. 2017], and foam-like [Martínez et al. 2016, 2017] structures, as well as two-dimensional, sheet-like materials [Leimer and Musalski 2020; Martínez et al. 2019; Schumacher et al. 2018; Tozoni et al. 2020]. While these previous works have explored many aspects of mechanical metamaterials, they all focus on elastic behavior. In contrast, we investigate a new class of metamaterials whose macro-scale behavior is regulated by internal contact, not elastic deformation.

*Homogenization.* The macromechanical properties of metamaterials can be determined using the toolset of homogenization theory [Bensoussan et al. 1978]. The central idea of homogenization is to infer macroscopic descriptions for the mechanical behavior of structured materials, typically by analyzing a representative patch of material subject to periodic boundary conditions. Most approaches use the same discretization (e.g., volumetric finite elements) for both native and macro scale simulation [Kharevych et al. 2009; Panetta et al. 2015; Schumacher et al. 2015]. Nevertheless, there are also cross-discretization approaches that map between very different computational models, e.g., from elastic rods to thin plates [Schumacher et al. 2018] or thin shells [Sperl et al. 2020]. Our method is likewise a cross-discretization approach, mapping from rigid body simulation to a 3D shell model. Unlike previous methods, however, we use homogenization to infer macroscopic deformation limits, not elasticity constants.

*Bi-Phasic Materials.* Capturing and modeling the behavior of elastic materials has a long history in graphics [Bickel et al. 2009; Hahn et al. 2019; James and Pai 1999]. An alternative to using highly nonlinear material models is to combine a weak elastic base material with deformation constraints [Goldenthal et al. 2007; Jin et al.

2017; Provot et al. 1995]. Whereas previous methods focused on edge-based strain limiting, Thomaszewski et al. [2009] suggested to enforce limits on per-triangle strain tensors, thus taking into account the full state of deformation. Wang et al. [2010] extended this concept to strain limiting based on singular value decomposition, which subsequent work applied to fully anisotropic limits on nonlinear deformation measures [Hernandez et al. 2013; Müller et al. 2015; Perez et al. 2013; Tang et al. 2022]. Our discrete interlocking materials can be considered an extreme case of bi-phasic materials: they initially show no resistance to deformation, but exhibit a hard stop once a limit is reached. However, instead of selecting deformation limits to approximate the behavior of highly nonlinear materials, we characterize materials by inferring deformation limits from native-scale simulation data.

*Simulating Contact.* Robust simulation of mechanical systems with frictional contact has been a core focus of graphics research for many years [Baraff 1989; Bertails-Descoubes et al. 2011; Erleben 2018; Geilinger et al. 2020; Hahn 1988; Kaufman et al. 2008; Li et al. 2022; Peiret et al. 2019]. We focus our survey on methods most relevant to interlocking assemblies with tight contacts. In this context, Qu and James [2021] propose a method that computes certificates for topological validity between arrangements of closed curves found, e.g., when simulating knitwear [Cirio et al. 2014; Kaldor et al. 2008] or chainmail. Robust time stepping with tight contacts is also the focus of Li et al. [2020], who propose smoothly clamped logarithmic barriers to guarantee intersection-free states at all times. Our native-scale simulation model builds on an extension by Ferguson et al. [2021] for intersection-free rigid body simulation. Building on data from this native-scale model, we propose a macro-scale simulation model that captures the high-level deformation behavior without the need to handle inter-element contacts.

*Interlocking Materials & Structures.* Using interlocking as a mechanism for creating stable assemblies is a concept that is used across architecture, robotics, and material sciences. For example, interlocking can be used to build functional furniture without nails or adhesives [Song et al. 2017; Yao et al. 2017], rigid assembly puzzles [Song et al. 2012; Wang et al. 2018; Xin et al. 2011], and stable surfaces made from flexible [Skouras et al. 2015] or rigid [Wang et al. 2019] components. Interestingly, imperfections during manufacturing can lead to loose joints such that assemblies, despite the rigidity of their components, can produce macroscopic deformations that can be harnessed, e.g., for robotics applications [Lensgraf et al. 2020].

Interlocking can also be used to create strong but flexible materials such as chainmail—a technique that has been known since ancient times. There are comparatively few works in material science and engineering that have revisited this technique. One example is the work by Engel and Liu [2007] who proposed a micro-machining process for creating chainmail-like fabrics. Ransley et al. [2017] combined a chainmail material with temperature controlled actuation for soft robotics applications. More recently, Wang et al. [2021] described a friction-modulated stiffening effect when subjecting sealed chainmail fabrics to external pressure. Our work uses the same material principle, i.e., periodic fabric-like arrangements of interlocking quasi-rigid elements. However, whereas Wang et al.

focus on elasticity as an emerging property, we address the fundamental question of quantifying the kinematic behavior of discrete interlocking materials.

### 3 COMPUTATIONAL MODEL

Our goal is to construct macroscopic descriptions for discrete interlocking materials (DIM) with a wide range of element shapes and topologies. To this end, we must first be able to predict the behavior of given DIM. We start by describing our native-scale model that simulates DIM on the level of individual elements (Sec. 3.1). We then use native-scale simulations to create macroscopic states of in-plane and out-of-plane deformations (Sec. 3.2). Using these macroscopic deformation tests, we construct a strain-space representation—the boundary between slack and taut regimes—that describes the space of feasible deformations for a given material. Finally, we propose a macro-scale simulation model that leverages this strain-space representation to efficiently predict the macromechanical behavior of DIM based on homogenized deformation constraints.

#### 3.1 Native-Scale Model

The mechanical behavior of Discrete Interlocking Materials is determined by the *shape* of their elements and the way in which they interconnect, i.e., their *topology*. By varying element shape and topology, a large range of macromechanical behavior can be obtained. Here we focus on quasi-rigid elements such that the mechanical behavior is entirely determined by kinematics—deformation limits—not elasticity. A natural choice to model this class of DIM is to represent individual elements as rigid bodies and model interactions between neighboring elements through contact forces. To predict deformation limits, we must compute static equilibrium configurations for given boundary conditions. We follow Ferguson et al. [2021] and cast rigid-body simulation with contact as an unconstrained minimization problem with logarithmic penalty functions that guarantee intersection-free states,

$$\min_{\mathbf{q}} E_{\text{Ext}}(\mathbf{q}) + E_{\text{Coll}}(\mathbf{q}), \quad (1)$$

where  $\mathbf{q} = (\mathbf{q}_1, \dots, \mathbf{q}_n)^T \in \mathbb{R}^{6n}$  is a vector holding six degrees of freedom  $\mathbf{q}_i = (\mathbf{x}_i, \boldsymbol{\omega}_i)$  for each of the  $n$  rigid elements, with  $\mathbf{x}_i$  and  $\boldsymbol{\omega}_i$  denoting center-of-mass positions and rotations, respectively. Furthermore,  $E_{\text{Ext}}(\mathbf{q})$  and  $E_{\text{Coll}}(\mathbf{q})$  are potentials due to gravity and contacts. We refer to [Ferguson et al. 2021] for details.

#### 3.2 Macro-Scale Deformations

The native-scale model allows us to study the response of DIM to arbitrary external forces. However, in order to describe these materials at a level of abstraction that is independent of the size and shape of a given sample, we must choose forces that lead to uniform macroscopic states of deformation. While we draw inspiration from homogenization theory for elastic media, the discrete nature of DIM requires a different approach as described next.

*In-plane Deformations.* To characterize the in-plane behavior of DIM, we first define a tileable unit cell as shown in Fig. 3(a). In order for this cell to be tileable, the positions of corresponding elements on opposite boundaries must be related by the same translation and

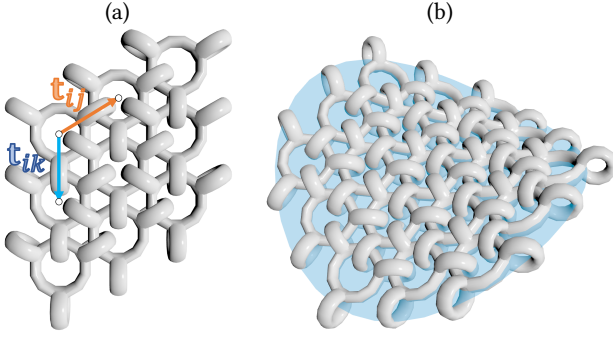


Fig. 3. Deformation limits for a three-fold symmetric material are probed in simulation using in-plane periodic boundary conditions (a) and paraboloid bending tests (b).

their orientations must match. For each boundary pair, these requirements lead to a set of *periodicity conditions* of the form  $\mathbf{x}_j = \mathbf{x}_i + \mathbf{t}_{ij}$  for translation and  $\boldsymbol{\omega}_j = \boldsymbol{\omega}_i$  for rotation. Analogous conditions are imposed for the second boundary pair, i.e.,  $\mathbf{x}_k = \mathbf{x}_i + \mathbf{t}_{ik}$  and  $\boldsymbol{\omega}_k = \boldsymbol{\omega}_i$ . Apart from enforcing tileability, these periodic boundary conditions can also serve for prescribing in-plane strains. For a given angle  $\theta$ , any such macroscopic strain can be defined through a principal direction  $\mathbf{d}_p = (\cos(\theta), \sin(\theta))^T$ , its orthogonal direction  $\mathbf{d}_o = (\cos(\theta + \frac{\pi}{2}), \sin(\theta + \frac{\pi}{2}))^T$ , and corresponding directional strains  $\boldsymbol{\varepsilon}_p$  and  $\boldsymbol{\varepsilon}_o$ . Given these quantities, we can define periodic translations for biaxial states of deformation as

$$\mathbf{t}_{ij} = \boldsymbol{\varepsilon}_p (\bar{\mathbf{t}}_{ij}^T \mathbf{d}_p) \mathbf{d}_p + \boldsymbol{\varepsilon}_o (\bar{\mathbf{t}}_{ij}^T \mathbf{d}_o) \mathbf{d}_o, \quad (2)$$

where the translations  $\mathbf{t}_{ij}$  and  $\bar{\mathbf{t}}_{ij}$  map vertices from one boundary to their counterparts on the opposite boundary in the current and reference configurations, respectively. The translation  $\mathbf{t}_{ik}$  for the second boundary pair is determined analogously, see Fig. 3. To draw a native-scale simulation towards a given macroscopic target strain  $\hat{\boldsymbol{\varepsilon}}$ , we solve the constrained minimization problem

$$\min_{\mathbf{q}, \boldsymbol{\varepsilon}} \frac{1}{2} (\boldsymbol{\varepsilon} - \hat{\boldsymbol{\varepsilon}})^2 + E_{\text{coll}}(\mathbf{q}), \quad \text{s.t. } \mathbf{C}_{\text{BC}}(\mathbf{q}, \boldsymbol{\varepsilon}) = \mathbf{0}, \quad (3)$$

where  $\mathbf{C}_{\text{BC}}(\mathbf{q}, \boldsymbol{\varepsilon})$  encode the periodic boundary conditions from (2) and  $\boldsymbol{\varepsilon} = (\boldsymbol{\varepsilon}_x, \boldsymbol{\varepsilon}_y, \boldsymbol{\varepsilon}_{xy})^T$ . Thanks to the coupling between strain variables  $\boldsymbol{\varepsilon}$  and element transformations  $\mathbf{q}$  through boundary conditions and collision penalties, this formulation ensures that strains remain valid even if target values are outside the feasible set.

*Out-of-plane Deformations.* To analyze deformation limits for bending, we initially consider using periodic boundary conditions analogous to the planar setting. While single curvature states—i.e., cylindrical bending—can be conveniently modeled in this way [Sperl et al. 2020], the concept of periodic boundary conditions does not readily extend to the doubly-curved setting: one cannot, in Euclidean geometry, define a finite-sized, double-curvature patch that tiles with itself [Sausset and Tarjus 2007]. Nevertheless, finite patches of DIM can generally assume states of double curvature. Some materials will even strongly resist uniaxial bending and prefer negative Gaussian curvature instead, see Fig. 2(b). For this reason, we lay aside periodic boundary conditions for out-of-plane behavior and instead

turn towards a penalty approach that *encourages* states of double curvature without strictly enforcing them through constraints. To this end, we define target surfaces with prescribed curvatures and ask that a given patch of interlocking elements should match this target as closely as possible. We use circular patches of paraboloid surfaces for this purpose, which are defined as  $z = Ax^2 + By^2 + Cxy$ . To achieve a given target curvature  $\hat{\boldsymbol{\kappa}}$ , we reparameterize the positions of all elements as  $\mathbf{x}_i(\boldsymbol{\kappa}) = (x_i, y_i, Ax_i^2 + By_i^2 + Cxy_i)^T$ , where  $\boldsymbol{\kappa} = (A, B, C)^T$ . We then find the feasible curvature closest to the target value by solving the minimization problem

$$\min_{\mathbf{q}, \boldsymbol{\kappa}} \frac{1}{2} (\boldsymbol{\kappa} - \hat{\boldsymbol{\kappa}})^2 + E_{\text{Coll}}(\mathbf{q}(\boldsymbol{\kappa})). \quad (4)$$

As in the planar setting, simultaneously optimizing for paraboloid parameters  $\boldsymbol{\kappa}$  and element transformations  $\mathbf{q}$  ensures that the corresponding curvature remains in the feasible set: any deviation would lead to intersections between elements, which are strongly penalized by the logarithmic penalty term  $E_{\text{Coll}}$ .

### 3.3 Strain-Space Representation

Having established the means to enforce macro-scale deformations for native-scale simulations, we can now start to build macromechanical representations of discrete interlocking materials. Unlike elastic materials, DIM can freely deform in a given direction until a hard stop due to tight contact between elements prevents further deformation. These deformation limits can vary strongly with direction and often depend on orthogonal deformations in highly nonlinear ways. To derive these limits, we observe that DIM can be fully described by enumerating all feasible macroscopic deformations. We assume that the set of all feasible in- and out-of-plane deformations forms a closed, simply-connected region in a six-dimensional strain space. While it is conceivable that materials violating this assumption can be constructed using, e.g., bi-stable/snap-through connections, we do not consider this case here. Even though bending and stretching deformations are coupled for the case of double curvature, our experiments and analysis indicate that treating in- and out-of-plane limits separately is a reasonable approximation (see Sec. 4.2). We, therefore, use distinct three-dimensional strain spaces for stretching and bending. See Fig. 4 for an example.

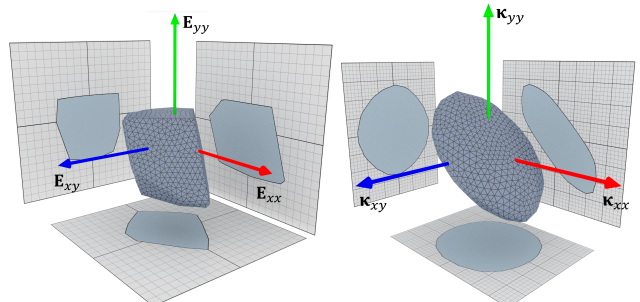


Fig. 4. Strain-space boundaries for the threefold symmetric chainmail material for in-plane (left) and out-of-plane (right) deformations. Projections of the 3D shapes onto strain-space planes are shown to improve readability.

**Stretching.** Planar states of strain form a three-dimensional space that can be parameterized in different ways. Using a canonical coordinate system with two axial stretches  $\epsilon_x$ ,  $\epsilon_y$ , and one shear strain  $\epsilon_{xy}$  is one possible choice. However, simple sampling strategies in this space will not lead to uniform distributions of samples with respect to the direction of deformation. For this reason, we parameterize planar strain through an angle  $\theta$  that transforms the canonical coordinate axes into the orthogonal directions of principal stretch. This system has zero shear strain such that two auxiliary variables  $\epsilon'_p$  and  $\epsilon'_o$  for stretch along the principal axes fully describe the planar state of strain as in Eq. (2). To explore the strain space boundary, we start by uniformly sampling directions  $\theta \in [0, \pi]$ . For each sampled direction  $\theta_i$ , we gradually increase (and decrease) the principal stretch  $\epsilon'_p$ . For each principal stretch value we then explore the limits of stretching and compression in the orthogonal direction. We always enforce zero shear to ensure that our principal strain coordinate system remains valid. Whenever we find a state for which deformation in either the principal or orthogonal direction cannot be further extremized, we have found a point on the boundary of the feasible set. In preparation for our macro-scale model, we then convert this point into its equivalent Green strain representation  $E = (E_x, E_y, E_{xy})^T$  in material coordinates and add it to the list of points used for constructing the strain space boundary.

**Bending.** To enable directional sampling of curvatures in analogy to the planar setting, we observe that any paraboloid with nonzero torsion  $C \neq 0$  can be reparameterized in terms of an angle  $\theta$  indicating the rotation of the canonical axes onto the directions of principal curvature. In this rotated system, we have nonzero curvatures  $A' \neq 0$ ,  $B' \neq 0$  but vanishing torsion  $C' = 0$  such that we can use the same boundary exploration strategy as for in-plane deformations.

**Strain-Space Representation.** The data generation strategy outlined above yields sets of points on the boundary between slack and taut regimes. We triangulate these point sets to obtain closed and watertight surface meshes that serve as explicit boundary representations  $\mathcal{B}_s$  and  $\mathcal{B}_b$  for stretching and bending, respectively. See also Fig. 4. Based on these strain-space boundaries, we define high-level directional deformation limits for characterizing discrete interlocking materials. We furthermore use these representations to construct macromechanical simulation models as explained next.

### 3.4 Macro-Scale Model

Native-scale simulation allows for accurate modeling and, consequently, analysis of the mechanical behavior of discrete interlocking materials. While the costs of native-scale simulation are acceptable for distilling macroscopic deformation limits from small samples, they become an impediment when exploring the behavior of larger assemblies. To enable efficient preview of DIM with larger numbers of elements, we develop a macro-scale model that combines thin-shell simulation with homogenized deformation constraints. To this end, we use the bending model by Gingold et al. [2004] as a basis, which provides direct access to curvature tensors using simple four-triangle elements. We complement this bending model using

linear triangle finite elements for in-plane deformations, which we quantify using the rotationally-invariant Green strain.

A key insight in this context is that we can enforce per-element stretching and bending limits as set inclusion constraints in strain space. Since the set boundaries are represented with triangle meshes, we can leverage established collision detection algorithms for modeling and enforcing strain-space constraints. To this end, we interpret per-triangle strain and curvature tensors as points in three-dimensional strain space. We enforce deformation limits through soft constraint functions that penalize the motion of points in strain space outside their boundaries  $\mathcal{B}_s$  and  $\mathcal{B}_b$ , respectively. Let  $s_i \in \mathbb{R}^3$  denote a point in strain space corresponding to the in- or out-of-plane deformation of triangle  $i$ . We first determine the distance  $d$  of  $s_i$  to the closest primitive—point, edge, or triangle—on  $\mathcal{B}$  using standard geometry tests and bounding volume hierarchies for acceleration. We then set up smooth, unilateral penalty functions as

$$E_{ss}(d) = \begin{cases} k_{ss}d^3 & d \geq 0 \\ 0 & \text{otherwise} \end{cases} \quad (5)$$

where positive distance values  $d \geq 0$  indicate points outside the strain-space boundary and  $k_{ss}$  is a penalty coefficient. We use the same strategy for defining penalty functions for stretching and bending limits, which are complemented by weak elastic potentials that regularize behavior inside the feasible region. For these regularizing materials, we aim to select stiffness coefficients that are large enough to prevent numerical problems, but small enough to not interfere with the deformation limits. To this end, we use a soft elastic base material with a Young's modulus of  $1250\text{Pa}$ , a Poisson's ratio of 0.4, and a mass density of  $250\text{kg/m}^3$ . To enable both implicit time stepping and static equilibrium simulation for our macro-scale model, we combine elastic and penalty potentials with an inertia term as described by Martin et al. [2011].

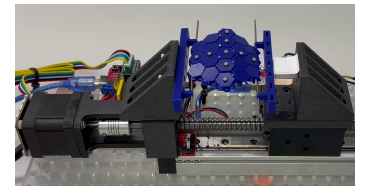
By reducing the number of variables and avoiding contact resolution at the element level, our macro-scale model is able to reduce computation times by one to two orders of magnitude compared to native-scale simulations. We present a detailed analysis of accuracy and computation times in Sec. 4.

## 4 RESULTS

We evaluate our method on a representative set of discrete interlocking materials and compare results obtained through simulation to measurements on physical prototypes. We start with a brief description of our experimental setup, after which we present our analysis of individual discrete interlocking materials.

### 4.1 Experimental Validation

For experimental validation, we fabricate sets of physical prototypes using 3D-printing. To obtain controlled deformation for both in-plane and out-of-plane motion, we



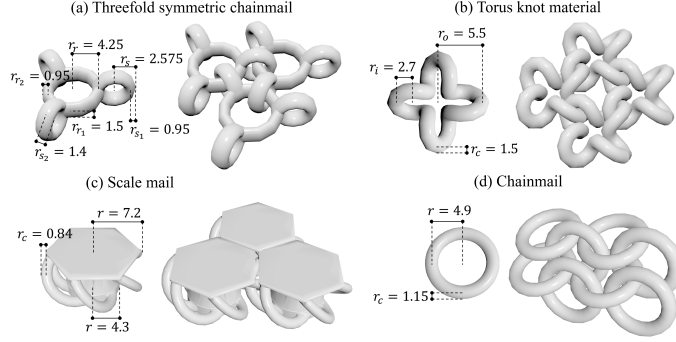


Fig. 5. Dimensions of elements (mm) and topology of interlocking for the materials considered in this work.

use a custom experimental setup as shown in the inset figure, consisting of a linear stage for precision actuation and a load cell for force measurement.

*In-plane Deformation Limits.* To experimentally identify the limits of the slack region, we stretch and compress samples along given directions until the load cell signals that a force threshold of  $2N$  has been reached. This process is repeated 5 times in each direction, and we report lower and upper bounds for the measurements in our plots.

These experiments result in a set of deformation limits for stretching and compression measured in absolute units of length. To remove dependencies on sample size and increase readability, we convert these limits into a Cauchy strain-like relative measure,

$$c = \frac{l_s - l_c}{l_c} = \frac{(1 + \varepsilon_s)L - (1 + \varepsilon_c)L}{(1 + \varepsilon_c)L} = \frac{\varepsilon_s - \varepsilon_c}{1 + \varepsilon_c}, \quad (6)$$

where  $l_s$  and  $l_c$  are the measured lengths for stretching and compression experiments. Visually, this directional Cauchy strain indicates the free range of travel relative to the corresponding minimal length under compression. Eq. (6) also shows that we can easily compute this metric from simulation data, with  $L$  denoting a reference length while  $\varepsilon_s$  and  $\varepsilon_c$  are corresponding stretch and compression limits. Summarizing strain values for different directions in a polar plot then enables direct comparison between experimental measurements and simulation data.

*Out-of-plane Deformation Limits.* We measure bending limits on physical prototypes using the same basic setup. To capture the state of curvature of a given sample, we additionally use an optical tracking system. To this end, we place markers on selected elements such as to sample both curvatures in principal and orthogonal directions. We then recover the closest state of constant curvature from the data by fitting circular arcs to the corresponding marker positions. We use the same experimental protocol as for the in-plane measurements. Due to the finite accuracy of our setup, however, we restrict bending tests to a smaller set of discrete directions that can be easily measured.

## 4.2 Analysis of Discrete Interlocking Materials

Our approach allows us to analyze a wide range of discrete interlocking materials. Here we show results for a set of four representative examples, illustrated in Fig. 5, that cover some of the major effects to be observed in these materials. For each example, we validate our method by comparing simulation results to measurements on physical prototypes.

*Threefold Symmetric Chainmail.* Our first example is the threefold symmetric structure shown in Figs 5(a) and 6(a). Each element of this material connects to its six immediate neighbors, leading to an overall threefold symmetric structure. As can be seen from Fig. 6(b), the material shows an almost isotropic limit profile for in-plane deformations with only small higher-frequency fluctuations. The simulation data is furthermore within the error bars (orange) of the experimental data. Here, the large discrepancy in the measurements is arguably due to displacements being small compared to the finite accuracy of our experimental setup. While the bending profiles under uniaxial bending shown in Fig. 6(c) and 6(d) are also almost isotropic, the difference in sign between principal and orthogonal curvature limits indicates a rather interesting coupling behavior: when applying uniaxial bending in any given direction, the material will bend with opposite curvature in the orthogonal direction, leading to characteristic saddle shapes as shown in Fig. 1(a). Interestingly, the amount of coupling seems to be determined by the aspect ratio of the elements' cross-sections. As shown in Fig. 2, ellipsoidal shapes induce hyperbolic curvature, whereas circular shapes lead to almost cylindrical bending. The limit plots are just a partial view onto the full set of kinematically-feasible deformations that is captured by our strain-space boundaries, shown in Fig. 6(e, f). These strain-space boundaries, which are best appreciated in the accompanying video, feed directly into our macro-scale simulation model, allowing us to predict the complex coupling behavior of this material in an accurate and efficient way. See Fig. 1(d).

*Torus Knot Material.* Our second example is a fourfold symmetric material consisting of torus knot elements arranged in a regular quadrilateral grid as shown in Fig. 5(b). As can be seen from the uniaxial strain plot in Fig. 6(b), this material exhibits almost isotropic in-plane limits, albeit with somewhat larger margins in 30 and 60 degrees. Compared to the threefold symmetric chainmail, however, these limits are much tighter. This material nevertheless admits significantly larger curvature, especially in 0 and 90 degrees. Interestingly, whereas this torus knot material only allows cylindrical curvature in 0 and 90 degrees, it admits doubly-curved states in 45 degrees. All of these observations can again be derived from the corresponding strain-space boundaries shown in Fig. 6(e, f).

*Scale Mail.* Our method can also be applied to elements with more complex geometry. In our third example, we consider a material made from elements with a sixfold symmetric base and a hexagonal plate on top of one side in Fig. 5(c)<sup>1</sup>. As can be seen from the uniaxial strain plot in Fig. 6(b), our simulation results are in good agreement with the measurements, showing a sixfold symmetric behavior with local maxima and minima for range of motion separated by 15

<sup>1</sup>This model is a modified version of the NASA chain mail material available at <https://www.thingiverse.com/thing:3095799>

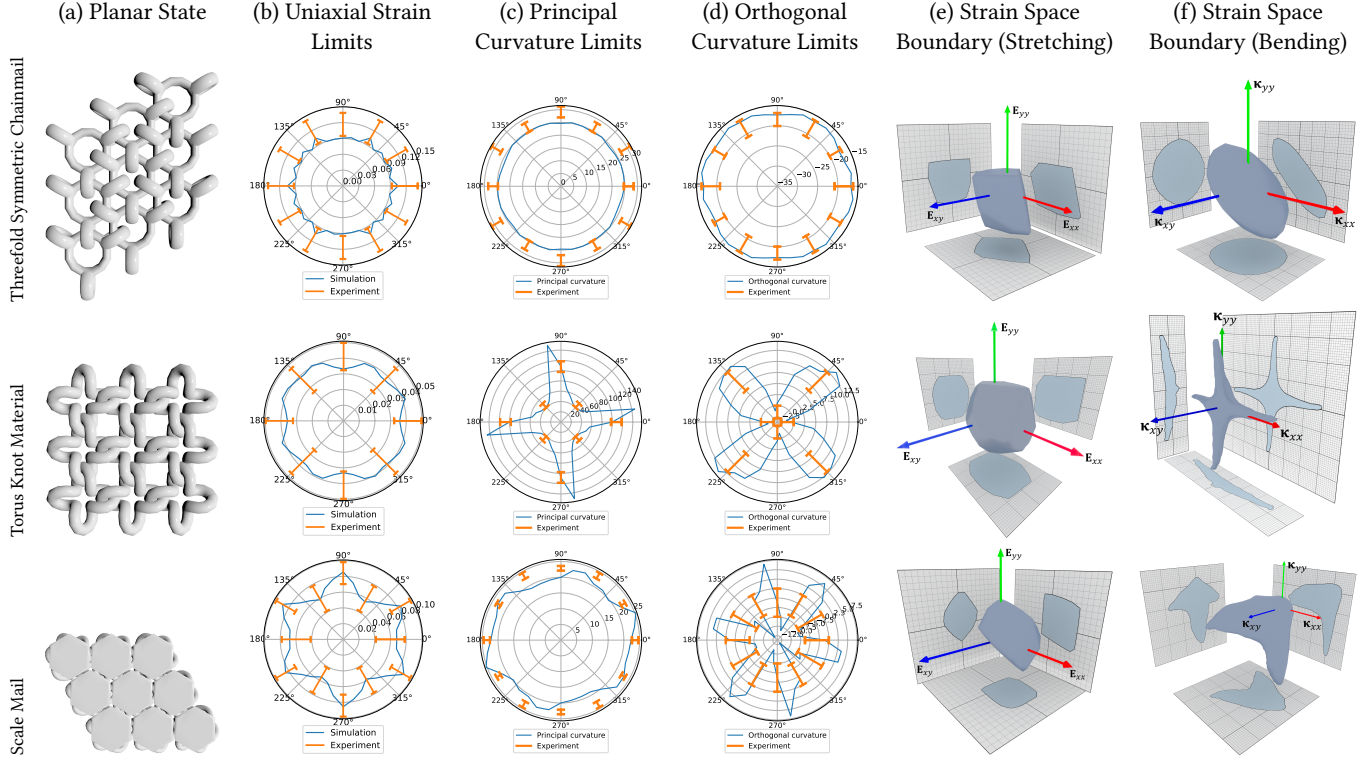


**Fig. 6. Deformations limits for threefold symmetric chain mail, torus knot, and scale mail materials.** Polar plots show directional deformation limits for uniaxial stretching (*b*) as well as biaxial curvature in the principal (*c*) and orthogonal (*d*) directions under uniaxial loading. For the uniaxial tests, we bend structures in a given principal direction until reaching their curvature limits. In the orthogonal direction, the structure is left free to deform under gravity and thus reaches a secondary curvature limit. We show the corresponding curvature limits in the principal (*c*) and orthogonal (*d*) directions. Solid curves (blue) correspond to simulation results which are sampled from  $[0, \pi]$  and rotated to fill the range  $[\pi, 2\pi]$ , experimental data is indicated using error bars (orange). These polar plots are partial views onto strain space boundaries for in-plane (*e*) and out-of-plane (*f*).

degrees. The curvature limits computed for this structure, shown in Fig. 6(*c, d*), show slightly larger deviations from the measurements but are still within acceptable margins.

Unlike all other materials considered here, this scale material is not symmetric through the thickness. This asymmetry in shape translates into an asymmetric bending behavior as shown in Fig. 12. For positive curvature, contact between the scales puts an early stop to bending. In the negative curvature direction, the bending limit is determined through contact between the interlocking rings and the base, which allows for much larger deformations. This peculiar asymmetric bending behavior can also be observed from the strain space boundaries shown in Fig. 6(*f*), which—unlike for the other materials—shows no symmetry with respect to curvature sign changes.

**4-in-1 Chainmail.** As our fourth example, we characterize the behavior of classic chainmail. This material is made of a staggered arrangement of ring-shaped elements that connect to their four immediate neighbors as shown in Fig. 5(*d*). As can be seen from Fig. 7(*b*), our simulation results for in-plane limits again show good agreement with experimental measurements. Although the range of travel for in-plane deformation is not substantially different from

other materials, this chainmail admits very large bending deformations. As shown in Fig. 7(*d*), the bending limits are indeed not determined by contact between directly connected elements but occur when remote elements come into contact upon folding. Since these folded configurations are far away from the constant-curvature case that we use for determining bending limits, our method cannot extract meaningful bending limits for this type of material. Nevertheless, accurate macro-mechanical behavior can still be obtained by combining the in-plane limits extracted from simulation data with a penalty-based collision handling approach such as IPC [Li et al. 2020].

**Discussion.** In summary, our method is able to capture the deformation limits for a wide range of discrete interlocking materials. In our analysis of different materials, we have identified several interesting phenomena, including strong coupling between bending modes as well as asymmetric bending limits. Although some of the results obtained through native-scale simulation may not align perfectly with experimental measurements, all of them can be deemed within acceptable margins. While many of the plots obtained from simulation data are smooth and symmetric, others exhibit imperfections and high-frequency fluctuations that are not in obvious

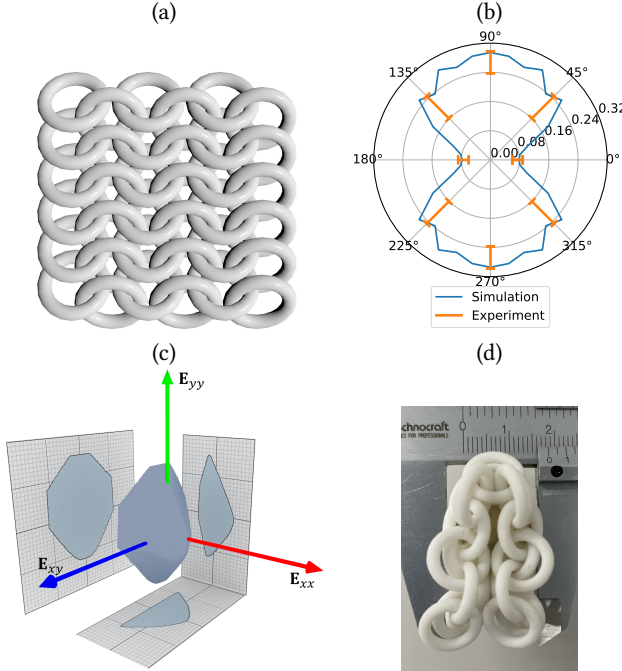


Fig. 7. 4-in-1 chainmail consisting of a staggered arrangement of rings, each of which connects to their four immediate neighbors (a). Deformation limits for uniaxial stretching (b) and strain space boundary for in-plane deformations (c). Bending limits are determined by contact between non-connected elements (d).

ways connected to the symmetry of the pattern. One explanation for such perturbations is the fact that in-plane strain is a function of the minimum length obtained for compressive loading. Compared to stretching, these compression tests are inherently more sensitive to noise, both in simulation and reality. Discrepancies between simulated and measured limits can also partly be attributed to the finite precision of our measurement setup. Bending tests generally showed much larger variations, which is arguably due to inaccuracies in marker placement, elastic deformations, as well as friction and gravity.

While our characterization of in-plane limits applies to arbitrary sample sizes, the same is not true for bending limits. As explained in Sec. 3.2, periodic tilings of doubly-curved patches do not exist in Euclidean geometry. Experimentally, however, we observe that finite sample sizes do admit double curvature. As shown in Fig. 8, our analysis of the relation between double curvature limits and sample size suggests that both principal and orthogonal curvature limits tighten with increasing sample size. We conjecture that this behavior is a direct consequence of Gauss's *Theorema Egregium*, i.e., the fact that nonzero Gaussian curvature inevitably leads to in-plane deformation. To see this, consider a given patch size with constant nonzero Gaussian curvature. Relative to its flat configuration, this patch must exhibit differential in-plane deformation, e.g., stretching at its center and compression along its boundaries. Increasing the patch size while maintaining the same Gaussian curvature, we

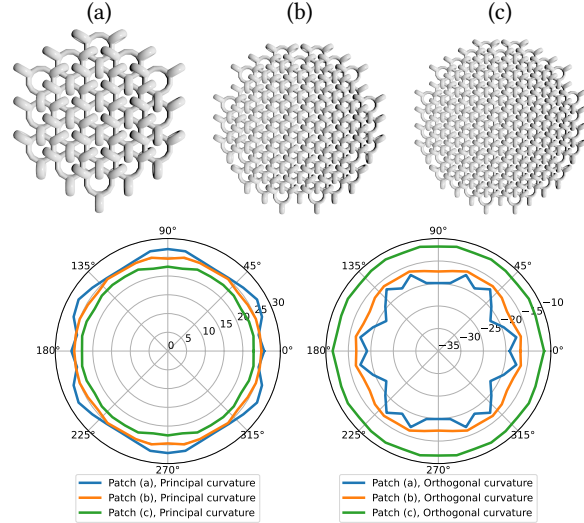


Fig. 8. Limits for double curvature depend on sample size. Absolute curvature values in both the principal and orthogonal directions decrease as patch size increases from 4 (a) to 6 (b) and 8 (c) elements along the diameter, corresponding to patch radii of 2.8cm, 4.8cm, and 5.8cm, respectively.

must either increase stretch at the center, or compression at the boundary—but both deformations are ultimately bounded by in-plane limits. Our conclusion from this observation is that in-plane limits, not bending limits, prevent double curvature states as sample size increases. We argue that, by measuring double curvature on smaller samples, our method nevertheless provides meaningful information on the intrinsic curvature preferences of discrete interlocking materials. Furthermore, our macro-scale simulations will automatically produce the effect of diminishing double curvature as sample size is increased even though we do not directly model coupling between in- and out-of-plane limits.

#### 4.3 Macro-scale Simulation

Having validated the deformation limits obtained through native-scale simulation and our strain-space boundary representation, we now evaluate the behavior of our macro-scale simulation model. All examples were run on a machine with an Intel Core i9-12900HK 2.5GHz processor and 32 GB of RAM.

*Comparison between Native- and Macro-Scale Simulations.* Using the materials analyzed in Sec. 4.1, we apply the strain space representations captured from native-scale simulation data to drive the deformation constraints in our macro-scale model. Fig. 9 shows a comparison between macro- and native-scale simulation results for the threefold symmetric chainmail, torus knot, and scale mail materials. For each material, we further compare results for different physical patch sizes. For native-scale simulations, we increase the number of elements according to patch size. For macro-scale simulations, we simply change the size of the mesh while keeping its resolution fixed. As can be seen from these comparisons, our macro-scale simulation results are in good agreement with their native-scale counterparts.

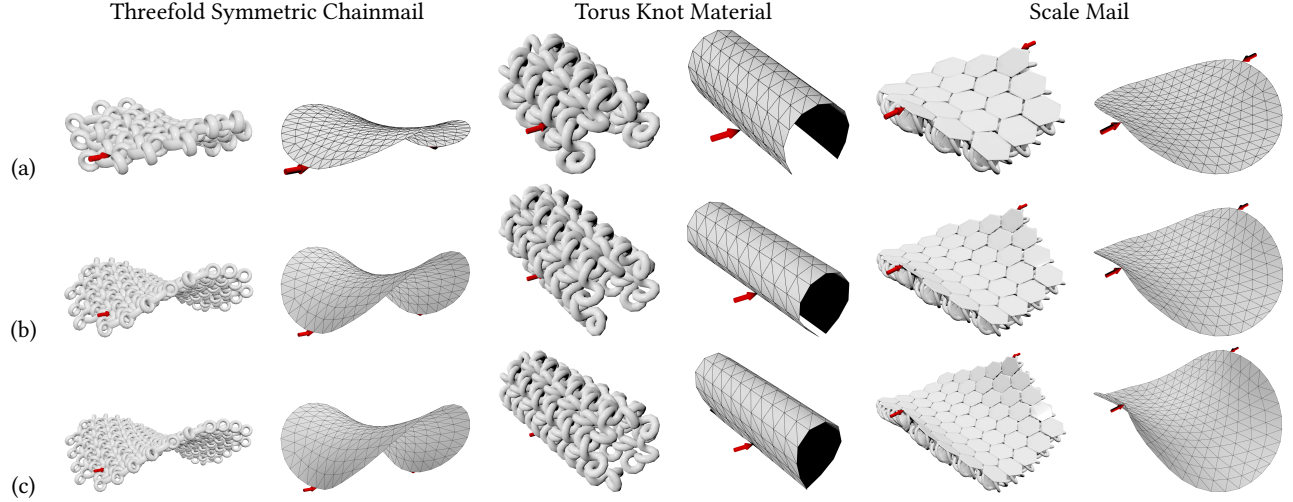


Fig. 9. Comparison between native- and macro-scale simulations for different materials. Static equilibrium states for applied point loads of 0.5N (red arrows) with different patch sizes. **Threefold symmetric chainmail**: we use disk patches of size 2.8cm (a), 4.8cm (b), and 5.8cm (c). Our macro-scale model uses the same resolution—but different physical sizes—of 384 faces and 217 nodes for all three cases. **Torus knot material**: we use patches with  $4 \times 4$  (a),  $5 \times 5$  (b), and  $6 \times 6$  (c) elements. Our macroscale model use again the same resolution ( $\#face = 200$ ,  $\#nodes = 121$ ) but different physical sizes with 4.4cm (a), 5.5cm (b), and 6.4cm (a) side length, respectively. **Scale mail**: we use disk-shaped patches with 19 (a), 37 (b), and 61 (c) elements and corresponding radii of 3.4cm, 4.6cm, and 5.9cm, respectively. Our macro-scale simulations use the same mesh resolution (384 faces and 217 nodes) for all patch sizes.

Table 1. Performance comparison between native- and macro-scale simulations for the examples shown in Fig. 9.

Example	Native-scale [s]	Macro-scale [s]	Speedup
Threefold (a)	133.526	68.394	2.0x
Threefold (b)	883.701	61.104	20.5x
Threefold (c)	1883.044	61.734	14.5x
Torus knot (a)	216.75	78.618	2.8x
Torus knot (b)	722.203	97.602	7.4x
Torus knot (c)	1647.41	141.261	11.7x
Scale mail (a)	179.057	43.581	4.1x
Scale mail (b)	962.517	36.821	26.1x
Scale mail (c)	4929.636	40.755	121.0x

As can be seen from Tab. 1, computation times for our macro-scale model are between one and two orders of magnitude smaller than for the native-scale model. It can further be noted that computation times for the native-scale model grow very rapidly with increasing problem size. Our macroscale model, however, shows almost constant cost since the same mesh resolution is used for all physical sample sizes. Small differences between macro-scale timings are due to the fact that more solver iterations are required to reach equilibrium states with larger deformations.

*Increasing Mesh Resolution and Young's Modulus.* To investigate the mesh dependence of our method, we compare macro-scale simulation results with increasing mesh resolution in Fig. 10. It can be seen that our macro-scale simulations behave consistently under refinement. We furthermore analyze the influence of the regularizing elastic material by comparing macro-scale simulation results for

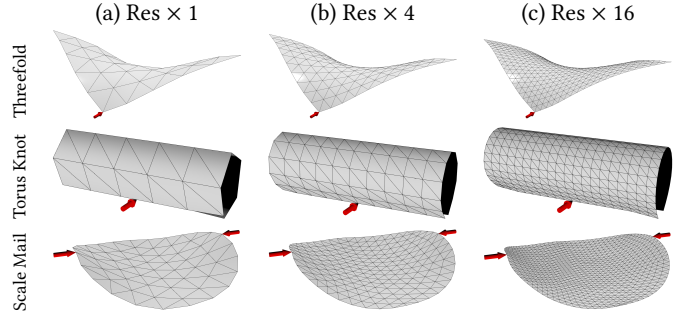


Fig. 10. Comparison of macro-scale simulation with increasing mesh resolution. We start from with coarse meshes (a) and increase resolution by a factor of 4 (b) and 16 (c).

increasing Young's moduli. From the results shown in Fig. 11, it can be seen that using too large a stiffness value (5000Pa) prevents the materials from reaching their deformation limits. It should be noted that the lower bound on the regularizing stiffness is determined by purely numerical considerations—below a certain stiffness, the linear solver will need additional diagonal regularization which slows down convergence, but the solution will be largely unaffected.

*Bending under Gravity.* As an additional test, we further analyze the ability of our macro-scale model to reproduce the asymmetric bending behavior of the scale mail material. To this end, we clamp one side of a hexagonal patch with 19 elements and let it deform into its equilibrium state under gravity. We then turn the sample upside down and repeat the experiment. As shown in Fig. 12, our macro-scale model captures the salient asymmetry in bending and

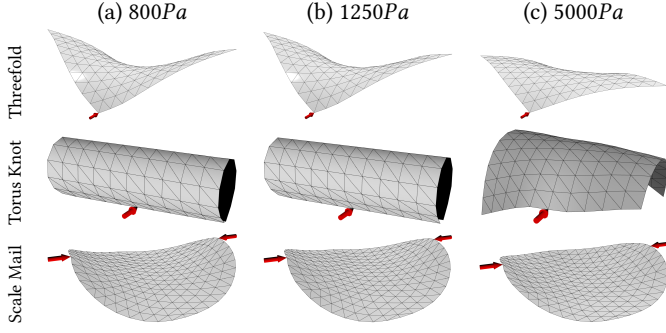


Fig. 11. Comparison of macro-scale simulations with increasing Young's Modulus.

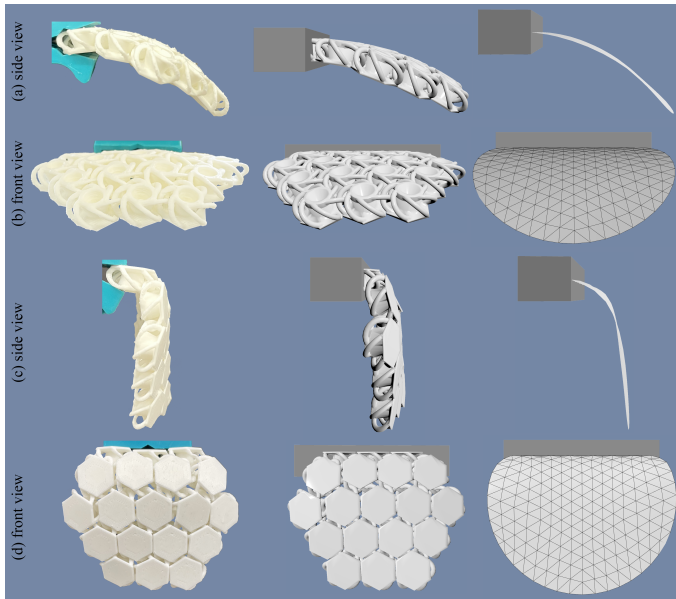


Fig. 12. **Asymmetric Bending Limits.** Due to the through-the-thickness asymmetry of its elements, this scale mail prototype (left) exhibits very different bending limits for positive and negative curvature. Our macro-scale model (right) accurately captures this behavior and closely tracks the native-scale simulation results (middle).

closely tracks the behavior of both native-scale simulation and the physical prototype.

**Constraint Violations.** We use penalty terms to enforce both in- and out-of-plane deformation limits. For all our macro-scale simulations, we use a stiffness coefficient of  $1e^7$  to ensure that constraint violation remains below 0.01%. To further analyze the accuracy of our macro-scale model, we investigate maximum constraint violations for the examples shown in Fig. 9. For each element, we compute the smallest positive distance between its corresponding point in strain space and the strain-space boundary. We normalize these values with respect to the diagonal length of the bounding box of the strain-space boundary and plot the maximum value as a

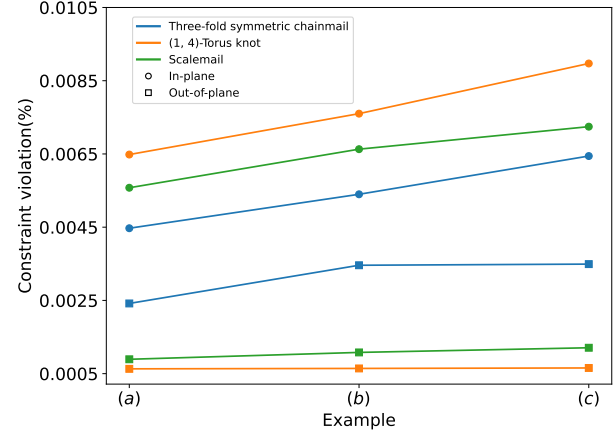


Fig. 13. Constraint violations for the examples shown in Fig. 9. Maximum constraint per-element constraint violations are plotted separately for in- and out-of-plane limits as indicated. It can be seen that constraint violations stay below 0.01% for all cases.

function of sample size. The results shown in Fig. 13 indicate that constraint violations are small for all cases.

## 5 CONCLUSIONS

We presented a method for computational modeling, mechanical characterization, and efficient macro-scale simulation of Discrete Interlocking Materials—generalized chainmail fabrics made from quasi-rigid elements. Unlike elastic materials, the mechanical behavior of DIM is governed by inter-element contacts that give rise to anisotropic deformation constraints. We proposed to explore these limits using thousands of native-scale simulations for in- and out-of-plane deformations. Using this simulation data, we have introduced the concept of strain-space boundaries as an explicit representation of the set of feasible deformations. These strain-space boundaries provide insight into the mechanics of DIM, and they also give rise to an efficient macro-scale simulation model based on homogenized deformation constraints. We have applied our method to a set of representative discrete interlocking materials and validated our findings against measurements on physical prototypes. We conclude that our methodology is well-suited for characterizing and modeling a broad range of discrete interlocking materials.

### 5.1 Limitations & Future Work

There are nevertheless several limitations of our work that indicate avenues for future work. Our analysis has focused on kinematic motion and, consequently, we have neither considered friction nor elastic deformations in the structure. While this approximation is justified for many types of discrete interlocking materials, friction forces can become dominant for tight materials in which elements have little freedom to move. Moreover, as shown by Wang et al. [2021], resistance to deformation can be controlled through normal pressure—a mechanism which crucially relies on friction. To apply our method to such friction-dominated scenarios, we would like to extend our macro-scale model to account for internal friction.

The work by Miguel et al. [2013] for modeling hysteresis in textiles through internal friction might be a good starting point.

While we modeled elements as rigid bodies, this is clearly an idealized assumption. None of our physical prototypes showed noticeable deformations for in-plane loading. For bending, however, an elastic regime can be *felt* for some of the materials. Modeling and characterizing elasticity of discrete interlocking materials outside the slack region is an interesting direction for future research.

Our method successfully captured the strain spaces for four different types of DIM using an increasing-and-decreasing biaxial loading scheme. Nevertheless, this simple scheme might not be able to fully explore strain spaces that are not star-shaped, i.e., for which rays from the origin can intersect the boundary more than once. We expect DIM with elements admitting twist or screw-like motions to fall into this category.

Our method offers an intuitive, systematic way for macromechanical characterization which can pave the way to using DIM for garment design. An interesting direction for future work would be to extend our formulation to inverse design problems such as finding element shapes that lead to desired deformation limits.

While strain space boundaries could perhaps be derived analytically for simple elements, obtaining closed-form deformation limits for complex-shaped elements seems elusive. Nevertheless, further analysis into the relation between structural symmetry and deformation limits is another exciting direction for future work.

Our macro-scale model offers a computationally efficient alternative that closely tracks native-scale behavior. However, our method does not provide geometric detail at the element level, which may be important for applications. Exploring mechanically-aware geometry synthesis and rendering methods in the spirit of Sperl et al. [2021] would be a worthwhile direction for future work.

Finally, while we have focused on homogeneous patterns with planar rest states, the space of possible discrete interlocking materials is much larger. In the future, we would like to explore the design and simulation of heterogeneous materials with curved rest shapes and spatially varying element shapes and connectivities.

## ACKNOWLEDGMENTS

We would like to thank Charles Gingras for the valuable discussion, and Ronan Hinchet for helping with the measuring setup and fabricating some of the physical prototypes. We are also grateful to the anonymous reviewers for their valuable comments. This work was supported by the Discovery Grants Program and the Discovery Accelerator Awards program of the Natural Sciences and Engineering Research Council of Canada (NSERC). Computing equipment has been funded through an infrastructure grant from the Canada Foundation for Innovation (CFI). This work was also supported by the European Research Council (ERC) under the European Union’s Horizon 2020 research and innovation program (grant agreement No. 866480), and the Swiss National Science Foundation through SNF project grant 200021\_200644.

## REFERENCES

- Moritz Bächer, Bernd Bickel, Doug L. James, and Hanspeter Pfister. 2012. Fabricating Articulated Characters from Skinned Meshes. *ACM Trans. Graph.* 31, 4, Article 47 (jul 2012), 9 pages. <https://doi.org/10.1145/2185520.2185543>
- D. Baraff. 1989. Analytical Methods for Dynamic Simulation of Non-Penetrating Rigid Bodies. *SIGGRAPH Comput. Graph.* 23, 3 (jul 1989), 223–232. <https://doi.org/10.1145/74334.74356>
- Alain Bensoussan, Jacques-Louis Lions, and George Papanicolaou. 1978. Studies in Mathematics and its Applications.
- Florence Bertails-Descoubes, Florent Cadoux, Gilles Daviet, and Vincent Acary. 2011. A Nonsmooth Newton Solver for Capturing Exact Coulomb Friction in Fiber Assemblies. *ACM Trans. Graph.* 30, 1, Article 6 (feb 2011), 14 pages. <https://doi.org/10.1145/1899404.1899410>
- Katia Bertoldi, Vincenzo Vitelli, Johan Christensen, and Martin Van Hecke. 2017. Flexible mechanical metamaterials. *Nature Reviews Materials* 2, 11 (2017), 1–11.
- Bernd Bickel, Moritz Bächer, Miguel A Otaduy, Hyunho Richard Lee, Hanspeter Pfister, Markus Gross, and Wojciech Matusik. 2010. Design and fabrication of materials with desired deformation behavior. *ACM Transactions on Graphics (TOG)* 29, 4 (2010), 1–10.
- Bernd Bickel, Moritz Bächer, Miguel A Otaduy, Wojciech Matusik, Hanspeter Pfister, and Markus Gross. 2009. Capture and modeling of non-linear heterogeneous soft tissue. *ACM transactions on graphics (TOG)* 28, 3 (2009), 1–9.
- Duygu Ceylan, Wilmot Li, Niloy J Mitra, Maneesh Agrawala, and Mark Pauly. 2013. Designing and fabricating mechanical automata from mocap sequences. *ACM Transactions on Graphics (TOG)* 32, 6 (2013), 1–11.
- Gabriel Cirio, Jorge Lopez-Moreno, David Miraut, and Miguel A. Otaduy. 2014. Yarn-Level Simulation of Woven Cloth. *ACM Trans. Graph.* 33, 6, Article 207 (nov 2014), 11 pages. <https://doi.org/10.1145/2661229.2661279>
- Stelian Coros, Bernhard Thomaszewski, Gioacchino Noris, Shinjiro Sueda, Moira Forberg, Robert W. Sumner, Wojciech Matusik, and Bernd Bickel. 2013. Computational Design of Mechanical Characters. *ACM Trans. Graph.* 32, 4, Article 83 (jul 2013), 12 pages. <https://doi.org/10.1145/2461912.2461953>
- Jonathan Engel and Chang Liu. 2007. Creation of a metallic micromachined chain mail fabric. *Journal of Micromechanics and Microengineering* 17, 3 (feb 2007), 551. <https://doi.org/10.1088/0960-1317/17/3/018>
- Kenny Erleben. 2018. Methodology for Assessing Mesh-Based Contact Point Methods. *ACM Trans. Graph.* 37, 3, Article 39 (jul 2018), 30 pages. <https://doi.org/10.1145/3096239>
- Zachary Ferguson, Minchen Li, Teseo Schneider, Francisca Gil-Ureta, Timothy Langlois, Chenfanfu Jiang, Denis Zorin, Danny M. Kaufman, and Daniele Panozzo. 2021. Intersection-free Rigid Body Dynamics. *ACM Transactions on Graphics (SIGGRAPH)* 40, 4, Article 183 (2021).
- Moritz Geilinger, David Hahn, Jonas Zehnder, Moritz Bächer, Bernhard Thomaszewski, and Stelian Coros. 2020. ADD: Analytically Differentiable Dynamics for Multi-Body Systems with Frictional Contact. *ACM Trans. Graph.* 39, 6, Article 190 (nov 2020), 15 pages. <https://doi.org/10.1145/3414685.3417766>
- Yotam Gingold, Adrian Secord, Han Jefferson, Eitan Grinspun, and Dennis Zorin. 2004. A Discrete Model for Inelastic Deformation of Thin Shells. In *Proc. of the ACM/Eurographics Symposium on Computer Animation (SCA) 2004 (Posters track)*.
- Rony Goldenthal, David Harmon, Raanan Fattal, Michel Bercovier, and Eitan Grinspun. 2007. Efficient Simulation of Inextensible Cloth. *ACM Trans. Graph.* 26, 3 (jul 2007), 49–es.
- David Hahn, Pol Banzet, James M Bern, and Stelian Coros. 2019. Real2Sim: Visco-elastic parameter estimation from dynamic motion. *ACM Transactions on Graphics (TOG)* 38, 6 (2019), 1–13.
- James K. Hahn. 1988. Realistic Animation of Rigid Bodies. In *Proceedings of the 15th Annual Conference on Computer Graphics and Interactive Techniques (SIGGRAPH ’88)*. Association for Computing Machinery, New York, NY, USA, 299–308. <https://doi.org/10.1145/54852.378530>
- Fernando Hernandez, Gabriel Cirio, Alvaro G Perez, and Miguel A Otaduy. 2013. Anisotropic strain limiting. In *Proc. of Congreso Español de Informática Gráfica*, Vol. 2.
- Doug L. James and Dinesh K. Pai. 1999. ArtDefo: Accurate Real Time Deformable Objects. In *Proceedings of the 26th Annual Conference on Computer Graphics and Interactive Techniques (SIGGRAPH ’99)*. ACM Press/Addison-Wesley Publishing Co., USA, 65–72. <https://doi.org/10.1145/311535.311542>
- Ning Jin, Wenlong Lu, Zhenglin Geng, and Ronald P Fedkiw. 2017. Inequality cloth. In *Proceedings of the ACM SIGGRAPH/Eurographics symposium on computer animation*, 1–10.
- Jonathan M. Kaldor, Doug L. James, and Steve Marschner. 2008. Simulating Knitted Cloth at the Yarn Level. In *ACM SIGGRAPH 2008 Papers* (Los Angeles, California) (*SIGGRAPH ’08*). Association for Computing Machinery, New York, NY, USA, Article 65, 9 pages. <https://doi.org/10.1145/1399504.1360664>
- Danny M. Kaufman, Shinjiro Sueda, Doug L. James, and Dinesh K. Pai. 2008. Staggered Projections for Frictional Contact in Multibody Systems. *ACM Trans. Graph.* 27, 5, Article 164 (dec 2008), 11 pages. <https://doi.org/10.1145/1409060.1409117>
- Lily Kharevych, Patrick Mullen, Houman Owhadi, and Mathieu Desbrun. 2009. Numerical coarsening of inhomogeneous elastic materials. *ACM Transactions on graphics (TOG)* 28, 3 (2009), 1–8.

- Kurt Leimer and Przemyslaw Musalski. 2020. Reduced-Order Simulation of Flexible Meta-Materials. *Proceedings - SCF 2020: ACM Symposium on Computational Fabrication*. <https://doi.org/10.1145/3424630.3425411>
- Samuel Lensgraf, Karim Itani, Yinan Zhang, Zezhou Sun, Yijia Wu, Alberto Quattrini Li, Bo Zhu, Emily Whiting, Weifu Wang, and Devin J. Balkcom. 2020. PuzzleFlex: kinematic motion of chains with loose joints. In *2020 IEEE International Conference on Robotics and Automation, ICRA 2020, Paris, France, May 31 - August 31, 2020*. IEEE, 6730–6737. <https://doi.org/10.1109/ICRA40945.2020.9196854>
- Minchen Li, Zachary Ferguson, Teseo Schneider, Timothy R Langlois, Denis Zorin, Daniele Panozzo, Chenfanfu Jiang, and Danny M Kaufman. 2020. Incremental point-to-point contact intersection and inversion-free, large-deformation dynamics. *ACM Trans. Graph.* 39, 4 (2020), 49.
- Yifei Li, Tao Du, Kui Wu, Jie Xu, and Wojciech Matusik. 2022. DiffCloth: Differentiable Cloth Simulation with Dry Frictional Contact. *ACM Trans. Graph.* 42, 1, Article 2 (oct 2022), 20 pages. <https://doi.org/10.1145/3527660>
- Lin Lu, Andrei Sharf, Haisen Zhao, Yuan Wei, Qingnan Fan, Xuelin Chen, Yann Savoye, Changhe Tu, Daniel Cohen-Or, and Baoguan Chen. 2014. Build-to-Last: Strength to Weight 3D Printed Objects. *ACM Trans. Graph.* 33, 4, Article 97 (jul 2014), 10 pages. <https://doi.org/10.1145/2601097.2601168>
- Sebastian Martin, Bernhard Thomaszewski, Eitan Grinspun, and Markus Gross. 2011. Example-Based Elastic Materials. *ACM Trans. Graph.* 30, 4, Article 72 (jul 2011), 8 pages. <https://doi.org/10.1145/2010324.1964967>
- Jonás Martínez, Jérémie Dumas, and Sylvain Lefebvre. 2016. Procedural voronoi foams for additive manufacturing. *ACM Transactions on Graphics (TOG)* 35, 4 (2016), 1–12.
- Jonás Martínez, Méline Skouras, Christian Schumacher, Samuel Hornus, Sylvain Lefebvre, and Bernhard Thomaszewski. 2019. Star-shaped metrics for mechanical metamaterial design. *ACM Transactions on Graphics (TOG)* 38, 4 (2019), 1–13.
- Jonás Martínez, Haichuan Song, Jérémie Dumas, and Sylvain Lefebvre. 2017. Orthotropic k-nearest foams for additive manufacturing. *ACM Transactions on Graphics (TOG)* 36, 4 (2017), 1–12.
- Eder Miguel, Rasmus Tamstorf, Derek Bradley, Sara C. Schwartzman, Bernhard Thomaszewski, Bernd Bickel, Wojciech Matusik, Steve Marschner, and Miguel A. Otaduy. 2013. Modeling and Estimation of Internal Friction in Cloth. *ACM Trans. Graph.* 32, 6, Article 212 (nov 2013), 10 pages. <https://doi.org/10.1145/2508363.2508389>
- Matthias Müller, Nuttapon Chentanez, Tae-Yong Kim, and Miles Macklin. 2015. Strain Based Dynamics. In *Proceedings of the ACM SIGGRAPH/Eurographics Symposium on Computer Animation* (Copenhagen, Denmark) (*SCA ’14*). Eurographics Association, Goslar, DEU, 149–157.
- Julian Panetta, Abtin Rahimian, and Denis Zorin. 2017. Worst-case stress relief for microstructures. *ACM Transactions on Graphics (TOG)* 36, 4 (2017), 1–16.
- Julian Panetta, Qingnan Zhou, Luigi Malomo, Nico Pietroni, Paolo Cignoni, and Denis Zorin. 2015. Elastic textures for additive fabrication. *ACM Transactions on Graphics (TOG)* 34, 4 (2015), 1–12.
- Albert Peiret, Sheldon Andrews, József Kövecses, Paul G. Kry, and Marek Teichmann. 2019. Schur Complement-Based Substructuring of Stiff Multibody Systems with Contact. *ACM Trans. Graph.* 38, 5, Article 150 (oct 2019), 17 pages. <https://doi.org/10.1145/3355621>
- Alvaro G Perez, Gabriel Cirio, Fernando Hernandez, Carlos Garre, and Miguel A Otaduy. 2013. Strain limiting for soft finger contact simulation. In *2013 World Haptics Conference (WHC)*. IEEE, 79–84.
- Xavier Provot et al. 1995. Deformation constraints in a mass-spring model to describe rigid cloth behaviour. In *Graphics interface*. Canadian Information Processing Society, 147–147.
- Ante Qu and Doug L. James. 2021. Fast Linking Numbers for Topology Verification of Loopy Structures. *ACM Trans. Graph.* 40, 4, Article 106 (jul 2021), 19 pages. <https://doi.org/10.1145/3450626.3459778>
- Mark Ransley, Peter Smitham, and Mark Miodownik. 2017. Active chainmail fabrics for soft robotic applications. *Smart Materials and Structures* 26, 8 (jul 2017), 08LT02. <https://doi.org/10.1088/1361-665X/aa7221>
- F Sausset and G Tarjus. 2007. Periodic boundary conditions on the pseudosphere. *Journal of Physics A: Mathematical and Theoretical* 40, 43 (oct 2007), 12873. <https://doi.org/10.1088/1751-8113/40/43/004>
- Christian Schumacher, Bernd Bickel, Jan Rys, Steve Marschner, Chiara Daraio, and Markus Gross. 2015. Microstructures to control elasticity in 3D printing. *ACM Transactions on Graphics (TOG)* 34, 4 (2015), 1–13.
- Christian Schumacher, Steve Marschner, Markus Gross, and Bernhard Thomaszewski. 2018. Mechanical characterization of structured sheet materials. *ACM Transactions on Graphics (TOG)* 37, 4 (2018), 1–15.
- Méline Skouras, Stelian Coros, Eitan Grinspun, and Bernhard Thomaszewski. 2015. Interactive Surface Design with Interlocking Elements. *ACM Trans. Graph.* 34, 6, Article 224 (nov 2015), 7 pages. <https://doi.org/10.1145/2816795.2818128>
- Méline Skouras, Bernhard Thomaszewski, Stelian Coros, Bernd Bickel, and Markus Gross. 2013. Computational design of actuated deformable characters. *ACM Transactions on Graphics (TOG)* 32, 4 (2013), 1–10.
- Peng Song, Chi-Wing Fu, and Daniel Cohen-Or. 2012. Recursive Interlocking Puzzles. *ACM Trans. Graph.* 31, 6, Article 128 (nov 2012), 10 pages. <https://doi.org/10.1145/2366145.2366147>
- Peng Song, Chi-Wing Fu, Yueming Jin, Hongfei Xu, Ligang Liu, Pheng-Ann Heng, and Daniel Cohen-Or. 2017. Reconfigurable Interlocking Furniture. *ACM Trans. Graph.* 36, 6, Article 174 (nov 2017), 14 pages. <https://doi.org/10.1145/3130800.3130803>
- Georg Sperl, Rahul Narain, and Chris Wojtan. 2020. Homogenized yarn-level cloth. *ACM Trans. Graph.* 39, 4 (2020), 48.
- Georg Sperl, Rahul Narain, and Chris Wojtan. 2021. Mechanics-Aware Deformation of Yarn Pattern Geometry. *ACM Trans. Graph.* 40, 4, Article 168 (jul 2021), 11 pages. <https://doi.org/10.1145/3450626.3459816>
- Ondřej Stava, Juraj Vanek, Bedřich Benes, Nathan Carr, and Radomír Měch. 2012. Stress relief: improving structural strength of 3D printable objects. *ACM Transactions on Graphics (TOG)* 31, 4 (2012), 1–11.
- Pengbin Tang, Stelian Coros, and Bernhard Thomaszewski. 2022. A Second Order Cone Programming Approach for Simulating Biphasic Materials. *Computer Graphics Forum* (2022). <https://doi.org/10.1111/cgf.14626>
- Bernhard Thomaszewski, Stelian Coros, Damien Gouge, Vittorio Megaro, Eitan Grinspun, and Markus Gross. 2014. Computational Design of Linkage-Based Characters. *ACM Trans. Graph.* 33, 4, Article 64 (jul 2014), 9 pages. <https://doi.org/10.1145/2601097.2601143>
- Bernhard Thomaszewski, Simon Pabst, and Wolfgang Straßer. 2009. Continuum-based Strain Limiting. *Computer Graphics Forum* 28, 2 (2009), 569–576.
- Davi Colli Tozoni, Jérémie Dumas, Zhongshi Jiang, Julian Panetta, Daniele Panozzo, and Denis Zorin. 2020. A low-parametric rhombic microstructure family for irregular lattices. *ACM Transactions on Graphics (TOG)* 39, 4 (2020), 101–1.
- Huamin Wang, James O’Brien, and Ravi Ramamoorthi. 2010. Multi-Resolution Isotropic Strain Limiting. *ACM Trans. Graph.* 29, 6, Article 156 (dec 2010), 10 pages.
- Yifan Wang, Liuchi Li, Douglas Hofmann, José E Andrade, and Chiara Daraio. 2021. Structured fabrics with tunable mechanical properties. *Nature* 596, 7871 (2021), 238–243.
- Ziqi Wang, Peng Song, Florin Iovoraru, and Mark Pauly. 2019. Design and Structural Optimization of Topological Interlocking Assemblies. *ACM Trans. Graph.* 38, 6, Article 193 (nov 2019), 13 pages. <https://doi.org/10.1145/3355089.3356489>
- Ziqi Wang, Peng Song, and Mark Pauly. 2018. DESIA: A General Framework for Designing Interlocking Assemblies. *ACM Trans. Graph.* 37, 6, Article 191 (dec 2018), 14 pages. <https://doi.org/10.1145/3272127.3275034>
- Shiqing Xin, Chi-Fu Lai, Chi-Wing Fu, Tien-Tsin Wong, Ying He, and Daniel Cohen-Or. 2011. Making Burr Puzzles from 3D Models. *ACM Trans. Graph.* 30, 4, Article 97 (jul 2011), 8 pages. <https://doi.org/10.1145/2010324.1964992>
- Jiaxian Yao, Danny M. Kaufman, Yotam Gingold, and Maneesh Agrawala. 2017. Interactive Design and Stability Analysis of Decorative Joinery for Furniture. *ACM Trans. Graph.* 36, 2, Article 20 (mar 2017), 16 pages. <https://doi.org/10.1145/3054740>
- Qingnan Zhou, Julian Panetta, and Denis Zorin. 2013. Worst-case structural analysis. *ACM Trans. Graph.* 32, 4 (2013), 137–1.
- Bo Zhu, Méline Skouras, Desai Chen, and Wojciech Matusik. 2017. Two-Scale Topology Optimization with Microstructures. *ACM Trans. Graph.* 36, 4, Article 120b (jul 2017), 16 pages. <https://doi.org/10.1145/3072959.3095815>
- Lifeng Zhu, Weiwei Xu, John Snyder, Yang Liu, Guoping Wang, and Baining Guo. 2012. Motion-guided mechanical toy modeling. *ACM Transactions on Graphics (TOG)* 31, 6 (2012), 1–10.